Earth Planet. Sci. Lett. 679 (2026) 119858

Contents lists available at ScienceDirect

Earth and Planetary Science Letters

journal homepage: www.elsevier.com/locate/epsl

Zircon deformation features reveal sequence of transient high stress, tension and shearing during seismic faulting: A case study from the Ivrea-Verbano Zone, Italy

Sandra Piazolo [a,*], Antonio Langone [b]

[a] School of Earth, Environment and Sustainability, Institute of Geophysics and Tectonics, University of Leeds, LS2 9JT, UK
[b] Department of Earth and Environmental Sciences, University of Pavia, Via Ferrata 1 – IT 27100 Pavia, Italy

ARTICLE INFO

Editor: Dr A Webb.

Keywords:
seismic faulting
Zircon
Crystal plastic deformation
Pseudotachylyte
Fragmentation
Micro-twin

ABSTRACT

The mechanisms associated with the propagation of fault ruptures remain debated in terms of sequence of events, processes and magnitude of stresses involved. Microstructures of zircon grains located within and in the immediate vicinity of pseudotachylyte veins reveal a sequence of events transient in time and space and allow recognition of different processes during rupture. The dynamic rupture causes, at its propagating tip, a damage zone of several centimetres thickness. In this damage zone, zircon grains exhibit crystal-plastic deformation signatures ranging from crystal lattice bending continuous throughout whole grains, to distinct planar deformation bands and {112} twin lamellae. Presence of planar deformation bands and {112} twin lamellae suggest locally high stresses, based on similar features reported from meteorite impacts. Absence of well-developed subgrains indicate dominance of low temperature plasticity at the rupture tip. Subsequently, those grains with highest dislocation densities undergo in-situ grain fragmentation. The observed correlation of grains with very high dislocation densities and in-situ grain fragmentation suggests that the effective tensile strength of these grains is sufficiently decreased by the high stored elastic energy to cause their fragmentation when subject to tensile stresses in the wake of the propagating rupture tip. Subsequent displacement along connected damage zone fracture surfaces results in pseudotachylytes formation.

Our data shows that dynamic rupture initiation and propagation results in stresses heterogeneously distributed in space, magnitude and sign causing both ductile and brittle deformation. Our study highlights the value of the accessory mineral zircon in deciphering the nature of rupture zone dynamics.

1. Introduction

Seismic slip within the lithosphere is an important mode of deformation with large repercussions for society (e.g. Scholz, 2002). However, the mechanism by which pseudotachylyte (rock formed by frictional melting) form within the ductile crust, below the seismogenic zone, remains debated (e.g. White 2012). There are two broad categories of mechanisms: (1) brittle processes thought to be directly related with dynamic rupture propagation (e.g. Raleigh and Paterson, 1965; Magloughlin, 1989; 1992; Spray, 2010; Okazaki and Hirth, 2016; Incel et al., 2019, Campbell and Menegon, 2022; Aldrighetti et al., 2025), and (2) ductile processes characterized by dissipative heating and thermal runaway situations (Braeck and Podladchikov, 2007; Kelemen and Hirth, 2007; John et al., 2009; Thielmann et al., 2015; Papa et al., 2018).

To resolve this debate, rocks that are interpreted to have undergone deformation associated with seismic signatures of earthquakes hold invaluable information. It is generally accepted that pseudotachylyte, a glassy or fine-grained fault rock, has undergone seismic slip as these have experienced frictional heat which is formed during seismic slip along planar fault zones (e.g. Sibson, 1975; Rowe and Griffith, 2015). Depending on the pseudotachylyte formation mechanism a different sequence of processes is expected before the pseudotachylyte forming seismic slip occurs. For ductile deformation significant shear deformation must occur prior to seismic slip. In contrast, wall-rock damage related to high stresses and strain rates at a propagating rupture tip is expected if brittle deformation is the dominant mechanism before frictional sliding, melting and pseudotachylyte formation occurs. Pulverization and fragmentation in the wall rock next to seismic faults is

* Corresponding author.
E-mail addresses: s.piazolo@leeds.ac.uk (S. Piazolo), antonio.langone@unipv.it (A. Langone).

https://doi.org/10.1016/j.epsl.2026.119858
Received 23 December 2024; Received in revised form 26 November 2025; Accepted 14 January 2026
Available online 22 January 2026

ubiquitous in the upper crust (Faulkner et al., 2011; Griffith et al., 2018). Since ductile deformation is more prevalent at high pressures and temperatures, it is expected that deep earthquakes are triggered by ductile deformation. However, there is growing evidence especially from a series of studies on dry, deep rocks exhibiting signatures of seismic slip have shown that this may not be the case (Austrheim et al., 2017; Incel et al., 2017; Menegon et al., 2017; Petley-Ragan et al., 2018; Jamtveit et al., 2018; Campbell and Menegon, 2022). The main argument for wall rock damage before rupture and pseudotachylyte formation (e.g. Petley-Ragan et al., 2018; Papa et al., 2020; Mancktelow et al., 2022; Aldrighetti et al., 2025) is the occurrence of highly distorted, fractured, fragmented and pulverized grains in direct vicinity of a pseudotachylyte. These features have been interpreted to be caused by the dynamic stress field associated with the propagation of the earthquake rupture. Minerals that have been shown to have undergone pulverization, fragmentation or intense fracturing in dry lower crust include plagioclase (Okudaira et al., 2017), clino- and orthopyroxene (Campbell and Menegon, 2022) and garnet (Austrheim et al., 1996; Austrheim et al., 2017: Petley-Ragan et al., 2018; Toffol et al., 2024). In an experimental study Incel et al. (2019) suggest that garnet grain pulverization is directly related to tensile stresses associated with dynamic shear rupture propagation. For the mid-crust, intense fracturing in direct vicinity to a pseudotachylyte vein has been observed in quartz and plagioclase (Aldrighetti et al., 2025). Based on quartz paleopiezometry and low temperature plasticity observations in pyroxene, preloading stresses in excess of 1GPa have been suggested (Campbell and Menegon, 2022; van Schrojenstein Lantman et al., 2025). We utilize microstructural features within a high number of zircon grains and their spatial relationship to a mid-crustal pseudotachylyte to track the sequence and nature of microphysical processes involved in earthquake rupture propagation and frictional melt generation and to assess the preloading stresses associated with seismic faulting in the mid crust. While high lattice distortions, and recrystallization in zircon have been linked to tectonic processes in mylonites (e.g. Piazolo et al., 2012, Kovaleva et al., 2014), the occurrence of {112} twin lamellae, transformation twins, phase transformation to the high-pressure phase reidite and granular texture have so far only been associated with meteorite impacts with hypervelocity compressional waves (e.g. Timms et al., 2017, Cavosie et al., 2015). Few studies explicitly discuss high stress deformation of zircon in a terrestrial, non-impact environment. Kovaleva et al. (2014, 2015) reported planar deformation bands (PDBs) and curvilinear fractures in zircon from pseudotachylytes and ultramylonites. They interpret that these formed during high stress and high strain deformation in the ductile field. This is contrasted by Austrheim and Corfu (2009) who link similar features to transient high stresses during rupture propagation.

Here we take advantage of deformation structures observed in the mineral zircon which is abundant within and in direct vicinity of pseudotachylyte veins. Different to studies on dry, plagioclase rich, lower crustal rocks, the rock studied here is a metagabbroic mylonite transected by a pseudotachylyte; both rock types are formed at mid-crustal, upper amphibolite facies conditions. The range of observed zircon microstructures suggest a high degree of stress heterogeneities during dynamic rupture propagation with stresses comparable, possibly even exceeding, those reported from dry rocks. Our large dataset allows us to determine that dynamic rupture propagation was followed by tensile stresses causing *in-situ* grain fragmentation which pre-date slip and frictional melting. Our data links high stored elastic energy within grains to their fragmentation suggesting that their effective tensile strength is surpassed during the transient tensile stresses in the wake of the propagating rupture even at medium to high confining pressures.

2. Geological background

The Ivrea-Verbano Zone (IVZ) of northwest Italy represents an uplifted part of the pre-Alpine middle to lower continental crust. Pseudotachylytes and a series of mid-crustal shear zones occur close to the Insubric Line (shear zones: e.g., Rutter et al., 1993; Langone et al., 2018; pseudotachylytes: e.g., Techmer et al., 1992; Pittarello et al., 2012; Fig. 1A). Faulting and shearing occurred during the early Mesozoic crustal extension (e.g., Pittarello et al., 2012; Ewing et al., 2015; Corvò et al., 2023; 2025). Pittarello et al. (2012) interpret the association of pseudotachylytes and ultramylonites as the result of repeated production of frictional melts due to downward propagation of seismic ruptures into the relatively water deficient metagabbros and granulites. Kovaleva et al. (2015) report planar microstructures in zircon in these shear zones suggesting that such structures represent an additional signature for high stress, high strain rate deformation. The studied pseudotachylytes stem from mylonitic to ultramylonitic metagabbroic rocks along a high-temperature shear zone exposed in Val Cannobina, IVZ (Fig. 1A, B). The Val Cannabina shear zone is part of a mylonitic to ultramylonitic belt developed within the 400–500m thick amphibole (±garnet) bearing metagabbro known as the External Gabbro (Figs. 1A, 1B; Langone et al., 2018). This mylonitic belt belongs to a network of high grade, Triassic-Jurassic fault zones such as the Anzola and Premosello shear zones (Fig. 1A, Corvò et al., 2023) where the formation of pseudotachylytes and ultramylonites occurred intermittently (Corvò et al., 2025). The metagabbro surrounds the mafic-ultramafic complex and the mantle peridotite of Finero (e.g., Tommasi et al., 2017) and is in contact with the metamorphic sequence of the Kinzigite Formation toward the SW (Fig. 1B, C) and exhibits pervasive brittle-ductile deformation features (e.g., Langone et al., 2018). Ductile deformation occurred mostly under amphibolite facies conditions ($T \geq 650°C$, $P \geq 0.6–0.4GPa$; Degli Alessandrini, 2018) and continued in distinct, localized zones under retrograde conditions during the exhumation related to the Late Triassic to Early Jurassic extensional tectonics (Langone et al., 2018; Corvò et al., 2023). The whole area has been subject to late brittle overprint during exhumation which manifests itself as a network of crosscutting fractures, mylonitic fabrics and pseudotachylyte veins.

3. Methods of analysis

Quantitative orientation analysis using electron backscatter diffraction analysis (EBSD)

To quantify local and mean geometrically necessary dislocation density (GND) we perform Weighted Burgers Vector analysis based on Wheeler et al. (2009, 2024) and now embedded in AztecCrystal3.2 (Oxford Instruments). It should be noted that the GND values derived from EBSD data are minimum estimates for the true dislocation density.

For further details of data acquisition see Appendix A (Supplementary Materials).

4. Results

4.1. General field and microstructural context

The studied samples exhibit a network of 1mm to 4cm thick pseudotachylyte veins which transect the mylonitic to ultramylonitic metagabbroic host rock (Figs. 1C, D; 2A, B; 3A). Rarely, exceptionally dark ultramylonitic layers are seen suggesting mylonitized former pseudotachylytes (Fig. 1E). Within a 2-5cm wide zone next to pseudotachylyte the host shows localized fracturing with μm-mm scale displacement and significant rotation (Figs. 1D, 2A,B, 3A) resembling a fracture related damage zone. The intact host (for details see Langone et al., 2018) and the damage zone are characterized by the presence of clinopyroxene, orthopyroxene, plagioclase (Fig. 2A,B,E) and locally brown amphibole (Fig. 2A). Within the damage zone, plagioclase is densely fractured (Fig. 2C) and shows clusters of 2-50μm fragments. Clinopyroxene exhibits local fragmentation and several sets of curved deformation bands filled with amphibole (Fig. 2D).

The pseudotachylyte matrix consists of a fine-grained granoblastic aggregate enveloping rounded/subrounded host clasts of single grains

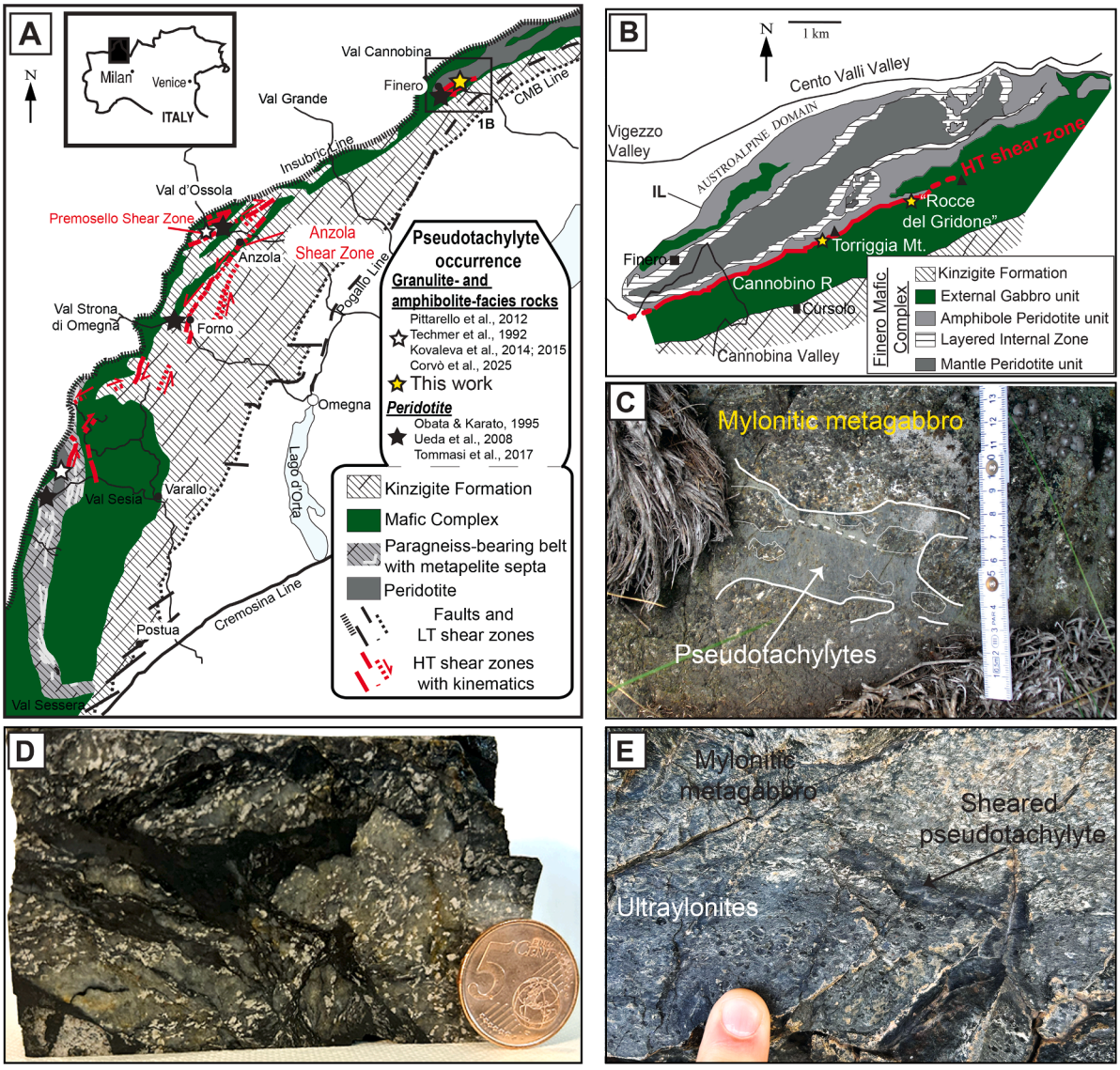

Fig. 1. Geological framework and outcrop characteristics. (A) Schematic geological map of the Ivrea-Verbano-Zone (IVZ; modified after Langone et al., 2018); l. The locations of high-temperature shear zones are after Rutter et al. (1993); stars indicate studied and reported pseudotachylytes locations were pseudotachylytes have been studied and/or reported (Obata and Karato, 1995; Tommasi et al., 2017; Ueda et al., 2008); yellow star this work. (B) Schematic map of the northern sector of the IVZ; the stars indicate the locations of studied pseudotachylytes. (C) Photo of one outcrop showing the relationship between pseudotachylyte and the host amphibolite facies, metagabbroic mylonitic metagabbro. (D) Photo of a sample slice highlighting the breccia-like pseudotachylyte studied. (E) Photo of studied one outcrop showing a sheared pseudotachylyte vein and dark ultramylonites.

or grain aggregates (Fig. 2E,H). Clasts commonly show rotation of the host mylonitic/ultramylonitic fabric (Fig. 3A). The clinopyroxene clasts are rimmed and welded by Ca-amphibole (Fig. 2G,H). Amphibole growth in the matrix and amphibole filled clinopyroxene deformation bands indicate amphibolite facies condition during pseudotachylyte formation, consistent with crystallization at mid-crustal levels. This is further supported by a lack of lower grade assemblages (chlorite, actinolite, epidote) in intact and mylonitized pseudotachylytes (Fig. 1E).

4.2. Zircon occurrence and general microstructural features

Zircon is abundant throughout the host rock, damage zone and pseudotachylyte (Figs. 2, 3, Appendix B, C and Figure S1). Their shapes and size vary from euhedral to anhedral and from 5 to 120μm, respectively (Figs. 2, 3). There are no systematic differences in zircon shape, size and aspect ratios with respect to their position in host, damage zone or pseudotachylyte (Fig. 3A, Appendix C). Under the optical microscope and in BSE images, zircon grains occur as (Fig. 3) (i) intact grains without internal fractures (Type I); (ii) internally fractured grains not showing relative shear offset of fragments (Type II); (iii) internally fractured grains showing shear offset of fragments (Type III). Type II and III grains closely resemble microstructures previously referred to shattered or pulverized minerals (e.g., Reches and Dewers, 2005; Austrheim et al., 2017). Intact grains occur throughout the whole samples. Fragmented grains with and without displacement are present in both pseudotachylyte veins and the damage zone, but absent in the intact host (Fig. 3B, Appendix B). Fragmented grains without significant displacement are seen dominantly within the fine-grained pseudotachylyte matrix (Fig. 3B, Appendix C).

Zircon types identified by BSE imaging do not correlate with particular CL characteristics (Figs. 3, 4, 6). For many grains CL zoning is weak or absent similar to CL characteristics described for the host mylonites (Langone et al., 2018; Appendix B). CL zoning may be overprinted by planar and curvilinear narrow bands (Fig. 4C; arrows).

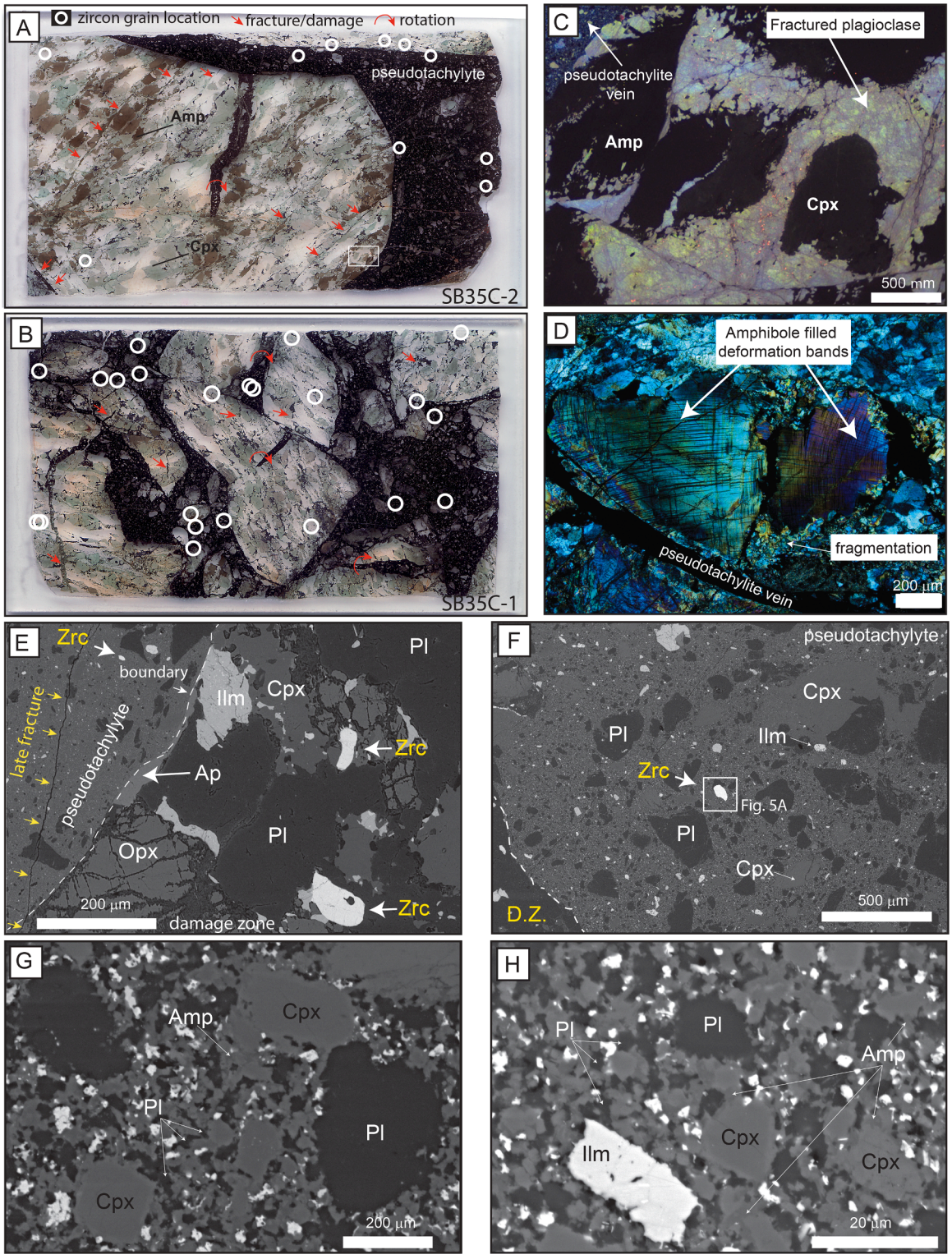

Fig. 2. General petrography and zircon locations. (A) & (B) Thin section overview of two typical samples with pseudotachylyte occurring as discrete veins (A; SB35C-2) and as breccia (B; SB35C-1); note white circles highlight zircon grains (white circles) (A) SB35C-2 (B) SB35C-3. (C) and optical microscope cathodoluminescence image showing high density of fractures in plagioclase adjacent to pseudotachylyte vein; location white box in (A). (D) Photomicrograph of clinopyroxene (CPX) grain in damage zone adjacent to a pseudotachylyte vein showing clear deformation bands which are filled with amphibole; cross polarized light. (E) BSE image of the boundary (stippled line) between pseudotachylyte vein and the damage zone showing the textural location of one zircon grain (Fig. 5A) within the fine-grained pseudotachylyte matrix; (F) BSE image of the boundary (stippled line) between pseudotachylyte vein and the damage zone (D.Z.) showing the textural location of two zircon grains within the damaged host rock and one within the fine-grained pseudotachylyte matrix; (G) and (H) BSE images of the granoblastic pseudotachylyte matrix showing plagioclase and clinopyroxene clasts and intergranular amphibole and plagioclase confirming amphibolite facies conditions during pseudotachylyte crystallization; note higher magnification of (H), bright spots of oxides and FeS and absence of lower grade minerals (e.g. epidote, actinolite). Cpx, clinopyroxene; Amp, amphibole; Opx, orthopyroxene; Pl, plagioclase; Zrc, zircon, Ilm, ilmenite.

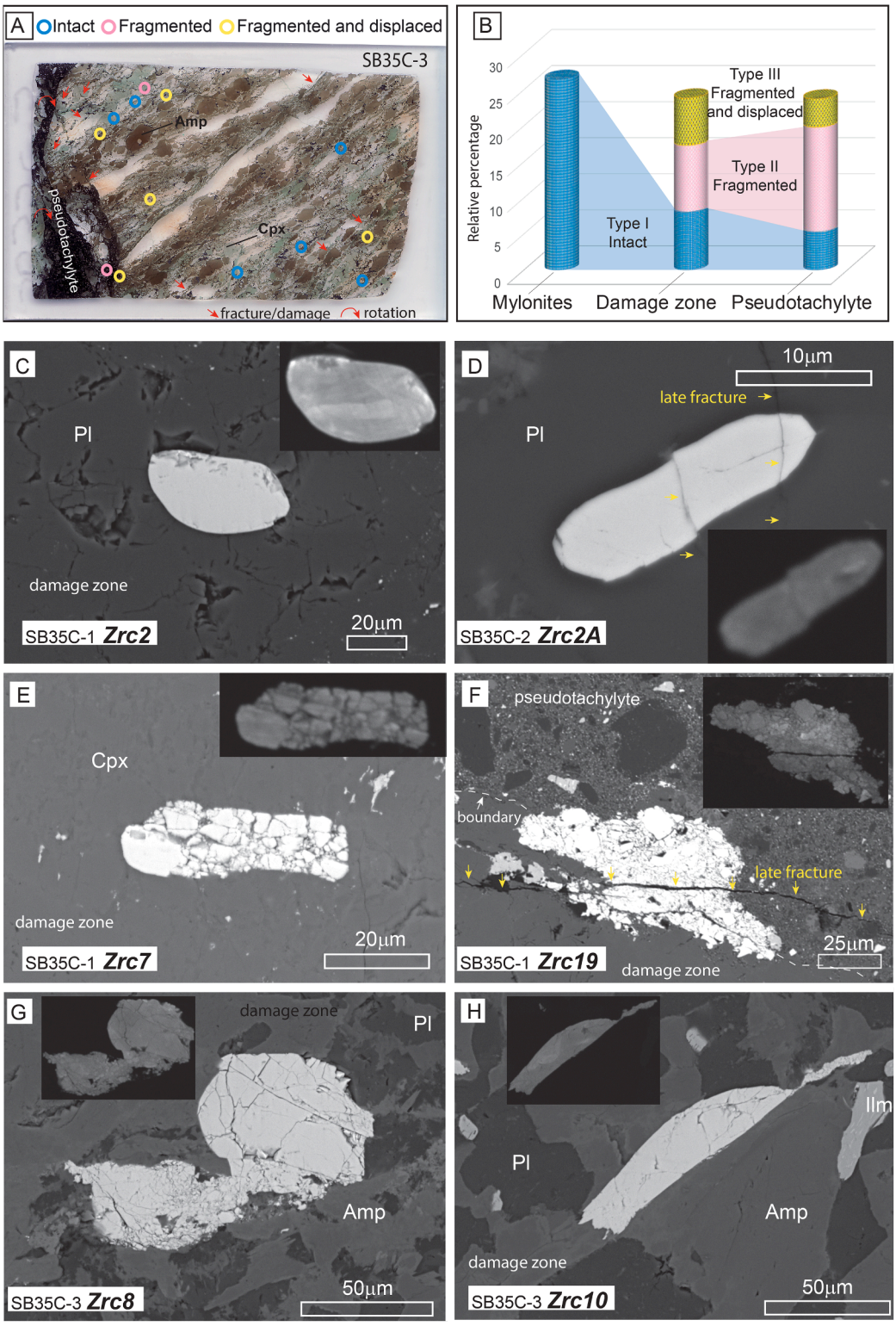

Fig. 3. General characterization of zircon grains. (A) Thin section scan of the sample SB35C-1 3 showing the location of zircon grains as circles colored according to their morphological features, i.e. intact (blue), fragmented (pink) and fragmented+displaced (yellow); see text for detailed definition; (B) histogram of the distribution of the intact, fragmented and fragmented+displaced zircon grains within the pseudotachylyte and the damage zone and host for the three analyzed samples; data provided in Appendix C (Supplementary Materials). (C)-(H) BSE images of zircon grains showing different features and within different textural position; insets show CL images. (C) Intact zircon included in plagioclase; SB35C-1 zrc2; (D) intact zircon grain with late (post-pseudotachylyte formation) fracture going through grain and the host rock;/mineral SB35C-2 zrc2A; (E) moderately fragmented grain within host; grain is within 50 micron of pseudotachylyte vein; SB35C-1 zrc7; (F) fragmented grain at the edge of the fine-grained pseudotachylyte matrix and host; note the late fracture cutting through host, pseudotachylyte and fragmented zircon (yellow arrows), SB35C-1 zrc19; (G) moderately fragmented grain in damage zone of host; SB35C-3 zrc8; (H) moderately fragmented grain with late displacement within the damage zone; SB35C-3 zrc10; also shown in Fig. 5C.

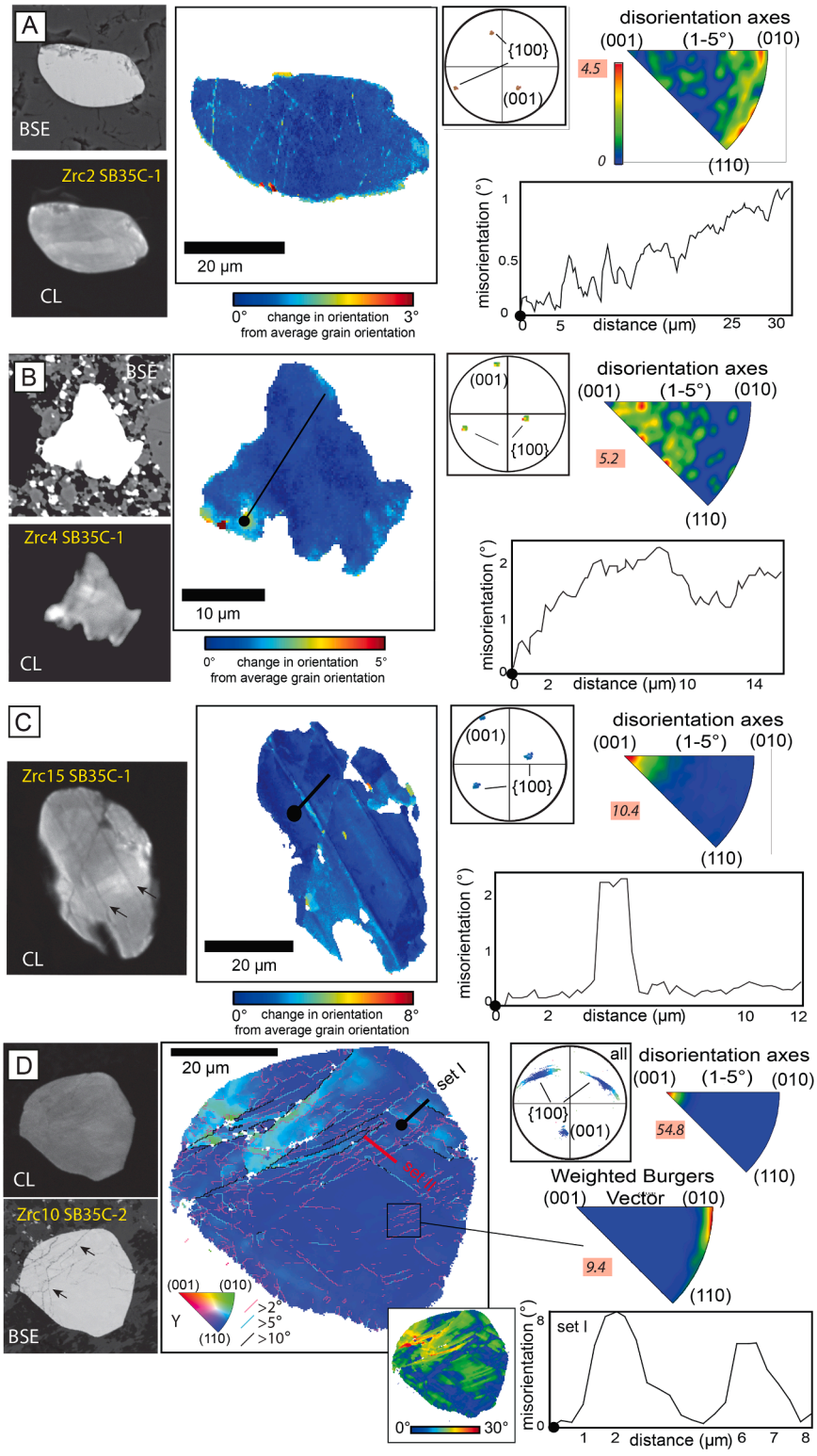

(caption on next page)

Fig. 4. Orientation relationships within representative geometrically intact zircon grains exhibiting low and intermediate lattice deformation; type I; step size 0.25mm; (left) BSE and CL images show position and internal structures, respectively; (A) example of very low lattice bending within fine grained matrix of pseudotachylyte vein; little change in seen in disorientation map (middle) while pole figure, misorientation profile and rotation axes (right) show little dispersions; SB35C-1 zrc2; (B) moderate deformation throughout zircon grain; BSE images shows position within fine grained matrix of pseudotachylyte vein; lattice bending depicted in the GROD disorientation map (middle), change in orientation by 0.2-0.5°/mm is shown in the misorientation profile (right bottom) while the pole figure and inverse pole figure of rotation axis of 1-5° illustrate a weak preference of rotation around c-axis (top right); SB35C-1 zrc4; (C) deformation with distinct deformation bands seen in CL (left, black arrows), disorientation map (middle), a clear rotation around <c> is seen in disorientation axes plot and pole figure (right top); deformation bands are characterized by clear changes along distinct band that are parallel to one (100); (D) highly deformed zircon grain with 2 sets of distinct deformation bands shown in CL image (top left) and in the orientation map (middle), disorientation profile shows the distinct nature of the deformation band (bottom right); large dispersion with rotation around <c> seen in pole figure and rotation axis diagram (top right); note the two sets of deformation bands are parallel to the two (100) planes shown in the pole figure; inset shows disorientation map (middle bottom) while BSE image shows grain boundaries forming within grains (black arrows); SB35C-2 zrc10.

4.3. Quantitative orientation analysis of zircon deformation features (1000)

Orientation analyses using EBSD combined with forescatter imaging were performed on zircon to assess the in-grain and intragrain deformation features. Grains from the damage zone, the pseudotachylytes and from the hosting mylonitic shear zone i.e., Val Cannobina (Langone et al., 2018; Appendix B1, B2), and the adjacent and coeval mylonitic belt, i.e., the Anzola shear zone (Corvò et al., 2023; Appendix B3) were analysed. EBSD analyses show that zircon grains exhibit a wide range of internal deformation microstructures that are only in part directly related to the optical microscopy, BSE based zircon types (Fig. 3B). Intact zircon (Type I) within the undamaged, mylonitic to ultramylonitic host show no to very little lattice distortion (Fig. 4A); they are similar to those observed in the adjacent mylonites and the Anzola shear zone (Appendix B). Only in rare cases, in mylonites and ultramylonites, curved high lattice distortions are locally seen along grain edges, suggesting indentation (e.g., Appendix B2_K; Piazolo et al., 2012; Kovaleva et al., 2014). In contrast, within the damage zone and pseudotachylyte, most intact Type I zircon grains show distinct deformation features (Fig. 4B, C, D); only a few zircons show a lack of lattice distortion (Appendix C). Deformation is manifested by continuous crystal lattice bending throughout a whole grain with no clear low angle boundary development (Fig. 4B). In rare cases, apparent low angle boundaries are observed; however, these are generally related to fractures. Internally, the change in lattice orientation is below 0.25°/μm. This is contrasted by distinct deformation bands bound by 2-8° boundaries, which are 1-3μm wide and several 10s of μm long (Fig. 4C,D). In these bands the lattice is similarly oriented on the two sides of the band and exhibit clear rotations around the <c> axis. Deformation band boundary orientations are planar and parallel to {100} planes (Fig. 4C,D). Several of these parallel bands can be observed in a single grain (Fig. 4C,D). Either one or two sets of deformation bands are observed. Some deformation bands form distinct fragments (Fig. 4D; arrows). Only in grains with such high lattice distortion subgrains are seen, however these are parallel to the deformation bands, curvilinear and show the same rotation axis dominance (Fig. 4D). In general, distortion becomes with increasing disorientation more systematic with the <c> axis as a rotation axis and clear continuous lattice distortions forming small circle dispersions, corresponding to a clear dominance of <010> Burgers vector (Fig. 4D, cf. Fig. 7B).

Fragments within the fragmented and fragmented and sheared zircon clusters (Type II and III) are clearly identified in BSE and forescatter images showing dominantly angular fragments ranging from <1μm to 10μm in size (Figs. 3 & 5). Fragments show in all cases significant internal crystal lattice distortion with the whole range of features outlined above. Fragmented but not displaced zircons can be subdivided into two subtypes. In the first group fragmentation is associated with relatively little change (1-8°) in orientation between fragments and clear crystal lattice bending that is systematic across the fragments (Fig. 5A). In contrast, in the second group grains show fragments that are highly misoriented relative to each other with orientation changes in the order of 10-60° (stars in Fig. 5B). Fragmented and displaced zircons exhibit post-fragmentation displacement or shearing, where fragments are displaced and show significant change in orientation from each other (Fig. 5C). Pole figures show less well-defined rotation axes, which is confirmed when plotting WBV in crystal coordinates which show a larger spread involving also <110> (cf. Fig. 7). This is most pronounced in the highly disoriented cluster (Fig. 5B).

In one grain clear {112} twin lamellae are present (zrc16A; Fig. 6). In addition, one fragment in a Type II grain cluster shows two parallel {112} twin lamellae (Fig. 5B; zoom-in). Zrc16A occurs at the boundary between the pseudotachylyte and the damage zone, it shows a main fracture with a small displacement (Fig. 6A). {112} twin lamellae are characterized by a 65° rotation around a common <110> axis while twin lamellae boundaries are parallel to a {112} plane (Fig. 6C). There are several parallel 0.2μm wide twin lamellae crossing the whole grain. Throughout the twin host high continuous crystal lattice distortion related to rotation around <001> mainly is seen (Fig. 6). Zrc16A is ~250 μm far from another zircon grain showing only lattice distortion and deformation bands but no {112} twin lamellae (Fig. 6A). No reidite or signatures of its former presence have been found.

4.4. Weighted Burgers Vector analyses

Geometrically necessary dislocation densities (GNDs) derived using Weighted Burgers Vector analysis (WBV; Wheeler et al., 2009; 2024) show a whole range of mean GND values correlating with the general classification of very low, low and moderate lattice bending, severely deformed, severely deformed and fragmented (Fig. 7A). Intact grains tend to exhibit relatively low mean GNDs, while fragmented grains are characterized by high to extremely high GNDs (Fig. 7A). High quality Electron Backscatter Patterns (EBSPs) taken from different grains show distinct, well-defined Kikutchi bands for low GNDs grains contrasting elastically distorted EBSPs for fragmented grains (insets Fig. 7A).

Type I, intact zircon grains from the Val Cannobina mylonites hosting the pseudotachylyte and from the Anzola shear zone exhibit low GNDs localized mainly at grain edges (Fig. 7A). In contrast GNDs in distorted Type I grains of the damage zone and pseudotachylytes are seen throughout grains and are often crystallographically controlled (commonly parallel to a low index planes) with distinct rotation axis and WBV preference (Fig. 4D, 7B).

WBV analysis shows a trend with increasing GND content where for intact grains WBV become well defined with a dominance of (010) (Fig. 7B, C). However, in highly fragmented zircon clusters GNDs are not only less organized spatially but also show a more pronounced spread of WBVs between (010) and (110) (Fig. 7D). The grain hosting {112} twin lamellae (Fig. 6D, red) has similar mean GND levels as severely deformed grains.

5. Discussion

5.1. Zircon microstructures reveal sequence of different microstructural features

The fact that outside the damage zone, zircon grains are intact and

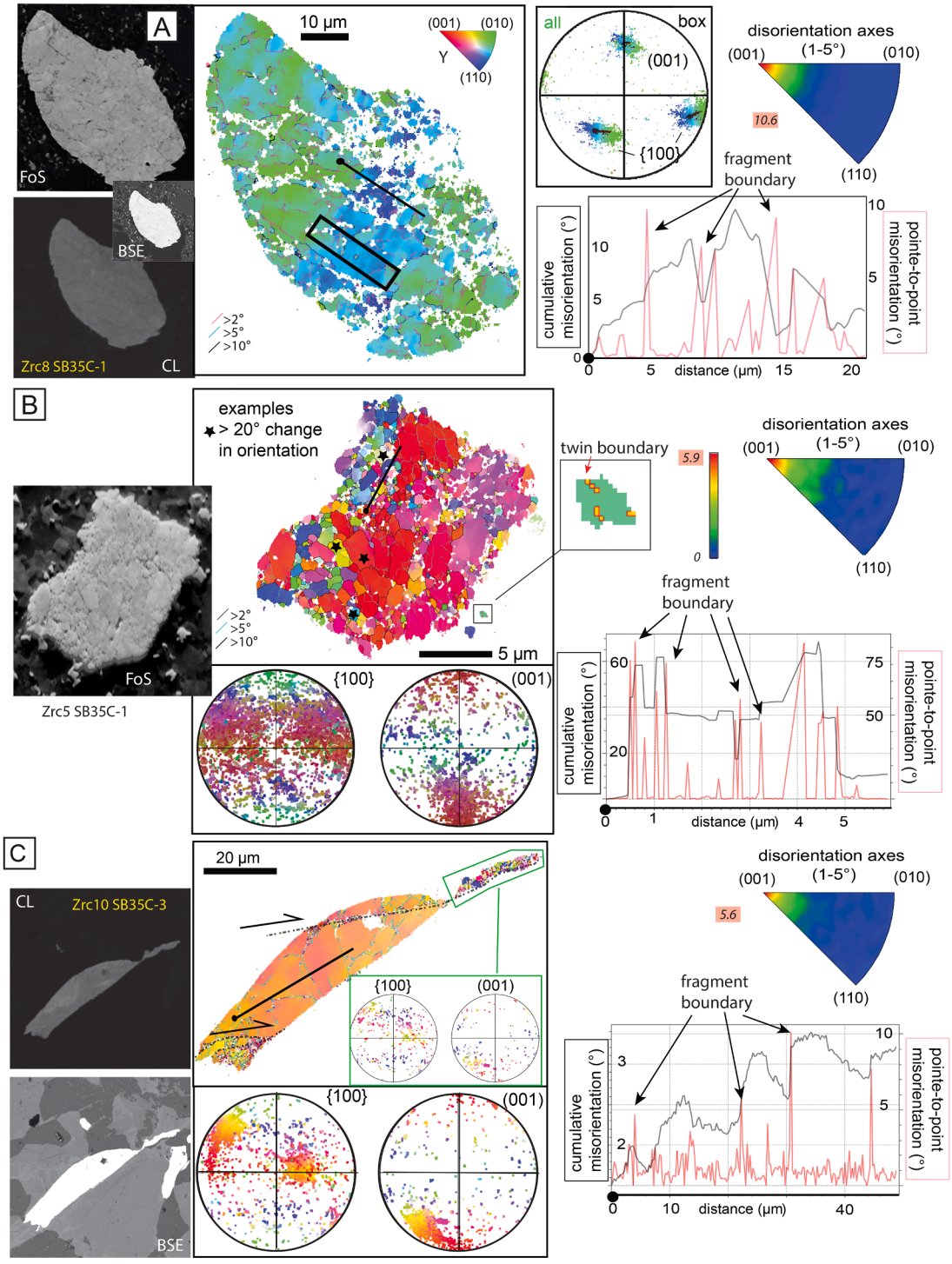

Fig. 5. Orientation relationships of representative zircon grains exhibiting different degrees of fragmentation and translation; type II and III; (A) type II, fragmented grain where fragments are clearly visible in the forescatter images (FoS), BSE and CL images, crystal bending within fragment is shown on orientation map (large map, centre) and pole figure; note large change in orientation over small area (subarea shown as black box in map and as black data in pole figure); misorientation change along black line shows orientation change along a the black line; (top left) rotation axis of data from subarea (black box). step size 0.25mm; SB35C-1 zrc8; (B) type II, fragmented zircon without displacement; shattering is seen clearly in the forescatter image (FoS); extreme dispersion of fragments in grain cluster is seen in the pole figures and orientation map; disorientation distribution graph shows high angles between fragments; zoom-in highlights one grain with {112} twin lamellae (see Fig. 6 for more details); (top left) shows rotation axis for low angles; step size 0.05mm; SB35C-1 zrc5; (C) type III; fragmented and displaced zircon showing little correlation between CL signature and orientation changes as shown on central orientation map; dispersion within the large grain is limited; material close to shear plane (stippled line in map) is dispersed; green box highlights late shear with associated pole figure (top left) shows rotation axis for low angles; step size 0.25mm; SB35C-3 zrc10.

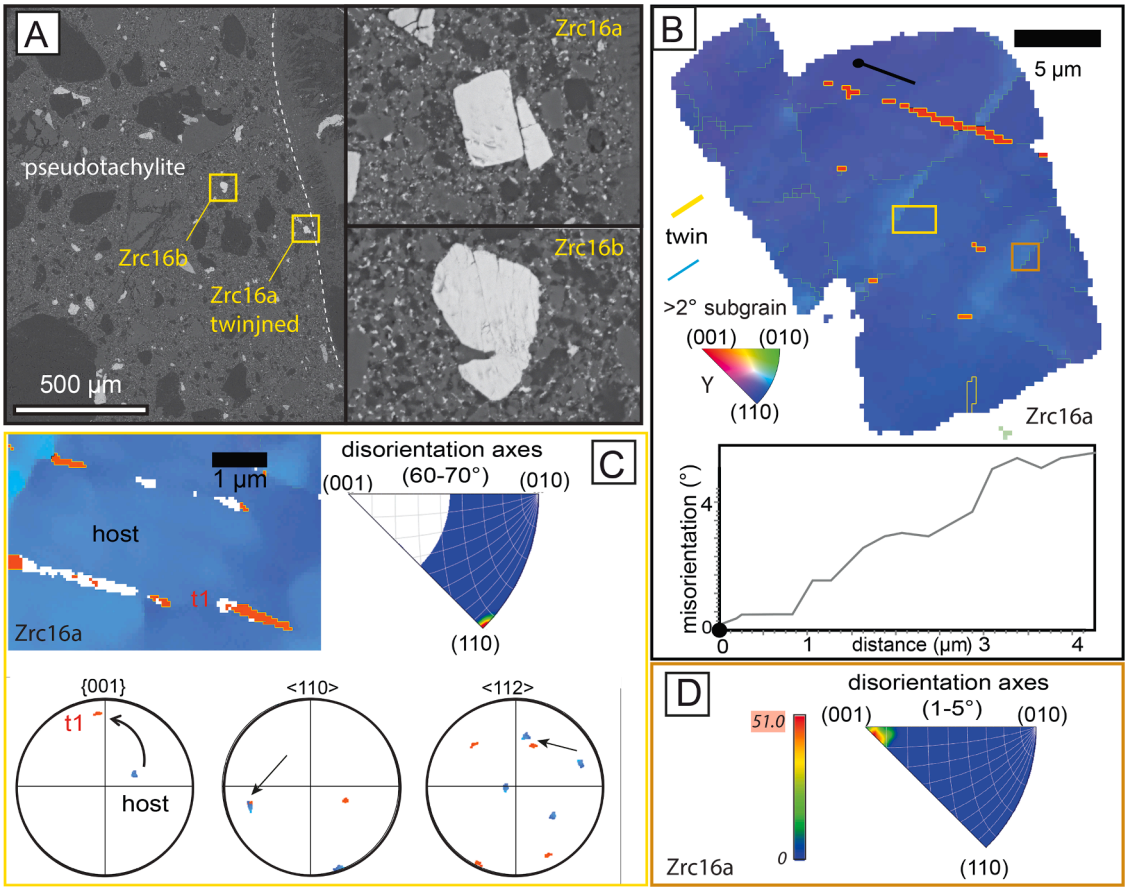

Fig. 6. Characterization of {112} twin lamellae; SB35C-1. (A) overview and close-up BSE images, showing position of two zircons within the pseudotachylyte vein; the twinned zircon (zrc16a) is close to the pseudotachylyte vein boundary (stippled line); the fragmented but non-twinned zircon (zrc16b) is further within the vein. (B) EBSD map showing crystallographic orientation changes in color (see legend) highlighting twin boundaries in yellow; significant lattice bending occurs within grain itself as shown by disorientation profile (see black line in map for location); step size 0.25mm. (C) (top) Zoomed-in orientation map (yellow box in (B)) with an inverse pole figure (IPF) color scheme showing a {112} shock-twin lamella; step size 0.05 mm; (bottom) Pole figures showing data zoomed-in map. Arrow in the {001} pole figure indicates apparent rotation of the twin from the host; arrows in the <110> and <112> pole figure indicate aligned pole of the host and twin; (D) low angle disorientation axes in crystal coordinates for characterizing in twin host grain distortion.

largely internally undeformed (Fig. 3B, Appendix C) suggests that deformation features within zircon observed must be directly related to the generation of the damage zone and/or pseudotachylyte formation. Not only grains outside the damage zone studied in the thin sections presented here, show a lack of significant crystal plastic deformation, but also zircon grains originating from the IVZ shear zones show the same lack of high lattice distortion (Fig. 7A, Appendix B). Their low degree of deformation both seen in EBSD lattice distortion maps (Fig. 4) and mean GNDs (Fig. 7A) is contrasted by zircons within the pseudotachylyte and damage zone which show a large range of deformation features, with only singular grains exhibiting no to little lattice distortion (Figs. 3B, 4, 5, 6, 7A). The fact that lattice distortions are disrupted by brittle structures contained in the zircons only, suggests that crystal plastic deformation occurred before brittle, grain bound deformation (Figs. 4D, 5A,B). Furthermore, some fractures coincide with distinct crystal lattice distortion features such as the curvilinear fractures and deformation band boundaries (e.g., Fig. 4D). This confirms deformation band generation before fracturing. The location of the different zircon types is not correlated with the position of the pseudotachylyte itself. Therefore, zircon types must have formed independent of the pseudotachylyte, hence prior to frictional slip. Consequently, the damage zone was formed and grains deformed and fragmented before fast slip along distinct planes occurred which resulted in pseudotachylyte formation. A similar relative timing of crystal plastic deformation, fragmentation and frictional slip resulting in pseudotachylyte formation is corroborated with the study by Campbell and Menegon (2022) who used pyroxene deformation features to determine the same relative sequence. Similarly, Austrheim et al. (2017), Petley-Regan et al. (2019), Mancktelow et al. (2022) and Aldrighetti et al. (2025) suggest fragmentation or intense fracturing at a propagating rupture tip followed by frictional sliding based on pulverized minerals, heavy fragmentation and fracturing at the wall-rock/pseudotachylyte interface. Incel et al. (2019) supported the latter interpretation by experimentally recreating the same microstructures and relative sequence. Kovaleva et al. (2014, 2015) studied zircon grains from a shear zone transect by pseudotachylytes and associated damage zones comparable to the shear zone object of this study (i.e., Premosello shear zone, Fig. 1A). The authors report highly distorted zircon grains suggesting that high zircon lattice distortions are related to damage zone formation, consistently with our interpretation.

We interpret these relative overprinting relationships to reflect transient events directly related to propagation of the earthquake rupture. As the rupture tip passes through the rock first local damage is caused along with zircon deformation, followed by fragmentation during tensile stresses while shearing behind the rupture tip causes rapid displacement resulting in frictional melting at the fault surfaces and thus pseudotachylyte formation. Details on these processes are discussed below.

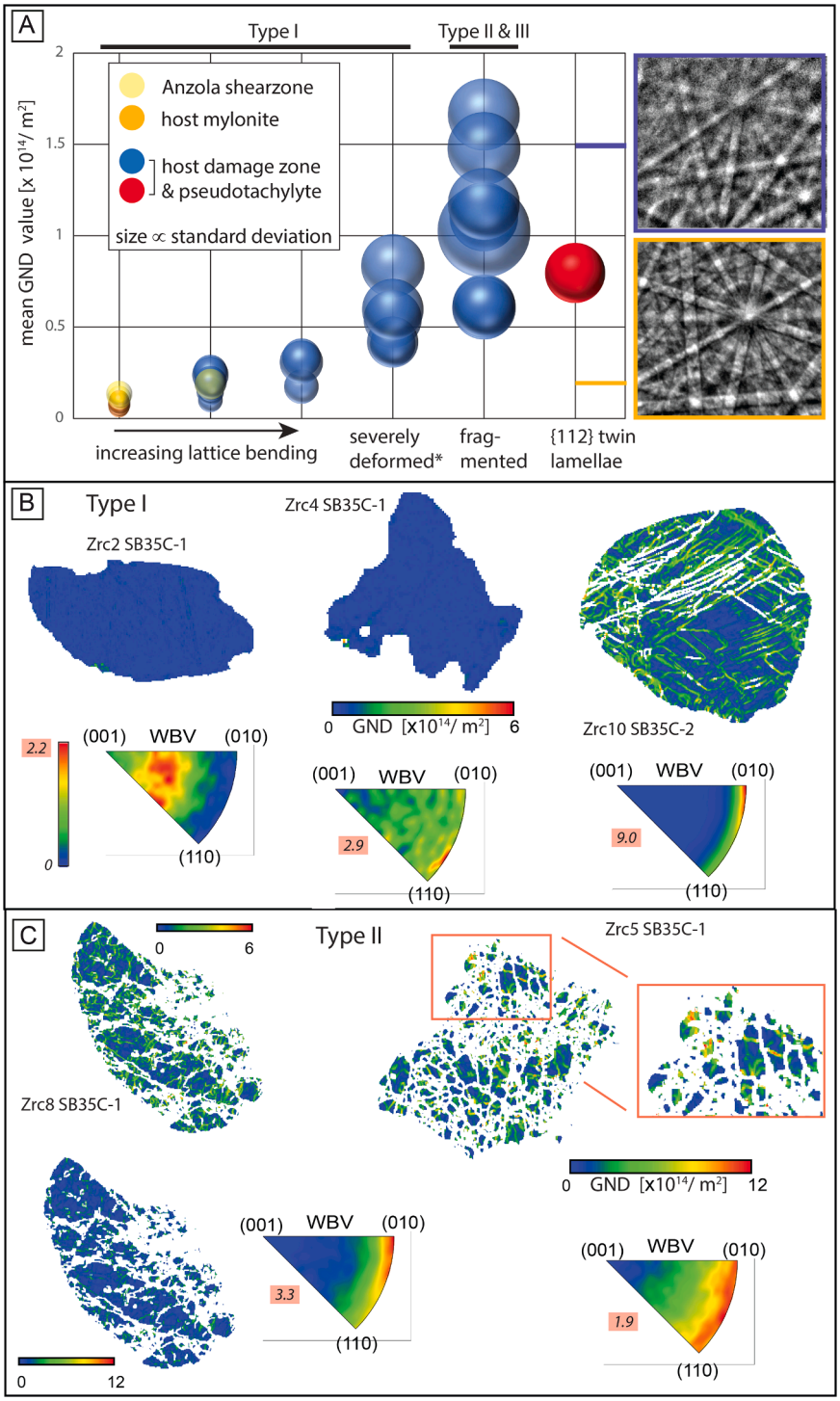

Fig. 7. Details on weighted burgers vector (WBV) and WBV derived GNDs within zircon grains; statistics and within grain variations; (A) statistics of mean WBV for different categories of grains i.e. Type I, II, III; size of the bubble is proportional to the standard deviation. Note the clear trend to very high dislocation densities for fragmented grains, with no distinction of fragmented and displaced versus fragmented only; *including grains with planar deformation bands (PDBs); orange and blue rimmed insets show electron backscatter patterns representative for grain with low mean GNDs and very high GNDs, respectively. (B&C) show GNDs value maps and WBV in crystal coordinate systems for angles $< 5°$ for type I and type II grains; respectively; note in C zoom-in.

5.2. Crystal plastic deformation features document local high stresses during dynamic rupture tip propagation

Crystal plastic deformation of zircon associated with systematic orientation changes of 0.5-2°/micron and low angle boundary development has been reported to be produced during regional tectono-metamorphic events (e.g., Kovaleva et al., 2014; Timms et al., 2006). The crystallographic character such as observed <001> axis as the rotation axis and boundary trace analysis suggest that documented crystal lattice bending is consistent with the dominant activation of the slip system <100>(010) which has been reported from high stress and strain rate shock experiments (Leroux et al., 1999) and from natural high strain rate deformation (Piazolo et al., 2012; Kovaleva et al., 2015). In samples undergoing regional style tectonic deformation, very high

crystal lattice distortion is only seen within a few 10s of micron of the zircon edges, suggesting that indentation of the zircon by other rheological hard grains is the cause (e.g., Reddy et al., 2006; Piazolo et al., 2012; Kovaleva et al., 2014). In these cases, distortions are closely related with the formation of 1-10° subgrain boundaries with plateaus of similar orientation in between. Some boundaries reach >10° disorientations. Such well-developed substructures suggest the activation of climb which is a diffusive process requiring sufficiently high temperature and/or slow strain rates to develop (e.g., Borthwick and Piazolo, 2010). This very localized but recovered lattice bending contrast those in our pseudotachylyte samples. We observe, lattice bending throughout whole grains (Figs. 4B,C,D, 5, 6). Subgrain boundaries of intermediate disorientations (5-10°) and subgrains without internal lattice bending (i.e. plateaus) are largely absent (Figs. 4, 5). High angle disorientations are generally associated with fractures observable in SE/BSE and forescatter images (e.g., Fig. 5). WBV analyses of grains with higher dislocation density show the activation of an additional slip system; here, <010> Burgers vectors are dominating, but an additional component of <110> is present, especially in high GND. The activation of another slip system suggests local higher stresses overcoming the higher critical resolved shear stresses necessary for slip on another slip system. High stresses are consistent with the observed distinct planar deformation bands (Fig. 4C, D). Such bands have been reported mainly from high stress/shock experiments from samples associated with meteorite impacts (e.g., Morozova et al., 2017; Jones et al., 2018; Timms et al., 2017 and references therein), except for Kovaleva et al. (2015) who related PDBs to high stress and strain rate in the ductile field.

Extremely high, instantaneous stresses are consistent with the presence of 0.1-1μm thick {112} twin lamellae with 65° disorientation about <110> and twin boundaries parallel with {112} in two studied grains (Figs. 5B, 6). Observed characteristics are identical to twin lamellae often referred to as shock-twins identified at several impact structures using EBSD, including Vredefort, Free State, South Africa (Moser et al., 2011; Erickson et al., 2013; 2017; Cavosie et al., 2015; Timms et al., 2017; Cox et al., 2018), Sudbury, Ontario, Canada (Thomson et al., 2014) and detrital shocked zircon interpreted as signatures of former impact structures (e.g., Montalvo et al., 2018). Importantly, these are not related to transformation twins that form from the back-transformation of the high pressure (>30GPa) zircon polymorph reidite (Timms et al. 2017). Shock pressures involve high deviatoric shear stresses in addition to extraordinary high mean stresses and twinning requires high resolved shear stresses on the twin plane in the twin direction (Trepmann 2008). In an impact breccia Trepmann (2008) found that mechanical Brazil twins in quartz formed at high differential stress rather than high shock pressures. Similarly, we interpret that the observed {112} twin lamellae are mechanical twins caused by shear stresses. Unfortunately, there is no experimental data to constrain the shear stresses for twin formation in zircon directly. So far, {112} twin lamellae have only been found experimentally in the run product of one static diamond anvil cell experiment that quenched zircon powder at 20GPa (Morozova et al., 2017). Based on evidence of crystal-plastic deformation of the twins, Morozova et al. (2017) suggest they may have formed at <11GPa marking the yield point of zircon. In addition, signatures for the activation of a secondary slip system caused by shear stresses has been observed in shock experiments at 4.5GPa (Fig. 7.5 in Morozova et al., 2017). Absence of reidite, presence of mechanical {112} twin lamellae together with the observed shift of WBV away from <010> towards <110> in the twinned grain (Fig. 6) and highly deformed grains (Fig. 5) points therefore to local high differential stresses. Based on the findings of Trepmann (2008) who showed that mechanical twinning occurred in samples devoid of microstructures indicative of high shock pressures, and the observed activation of a secondary slip system, we suggest the presence of mechanical {112} twin lamellae and two slip system activation in zircon indicate shear stresses on the order of a few GPa. This is consistent with the nature of propagating rupture dynamics where very high differential stresses in the vicinity of the propagating tip are expected (Reches and Dewers, 2005). We caution that the suggested shear stress estimate of a few GPa is indicative only as it is drawn from the impact related shock pressure literature. To derive reliable preloading stress estimates related to fault ruptures in tectonic settings linking microstructures to stresses additional dedicated experiments are needed. In the absence of such experiments still some conclusions may be drawn. Our indicative stress estimate supports the stresses in the order of 1GPa recorded by diopside deformation within dry, deep rocks (Campbell and Menegon 2022; van Schrojenstein Lantman et al., 2025). Importantly, our data extends zircon deformation microstructures associated with tectonic deformation to {112} twin lamellae. Stresses must have been highly heterogeneous based on the observed high variability in the degree of observed crystal lattice distortion and up to 2 orders of magnitude difference in GNDs within zircon. Such heterogeneity is expected as the rock studied is polycrystalline and polymineralic where local stresses may vary by 1-2 orders of magnitude based on its heterogeneity in physical properties of their components. Even in monomineralic polycrystalline materials like ice, stress variability of 1 order of magnitude has been shown (e.g., Piazolo et al., 2015).

5.3. *High dislocation density results in a decrease of tensile strength allowing in situ fragmentation of highly deformed zircon*

The observed fragments of fragmented zircon without significant displacement are separated by clear fractures seen in SEM images (Figs. 3-5). Fragmentation of different minerals with clear fracture surfaces has been already described within host rocks of shallow faults (e.g., Trepmann and Stöckhert, 2002; Doan and Gary, 2009). There is growing evidence for fragmentation in direct vicinity of pseudotachylyte veins and survivor clasts within pseudotachylytes in deep crustal rocks (e.g., garnet: Austrheim et al., 1996, 2017; Incel et al. 2019; pyroxene: Campbell and Menegon, 2022). Papa et al. (2018) reported garnet extremely comminuted "*in situ*" (without any displacing cataclastic flow) from amphibolite-facies metapelites. Two main hypotheses have been put forward for this *in situ* shattering: (1) *In situ* shattering of minerals in contact with pseudotachylytes occurred after the formation of frictional melt related to the thermal shock induced fragmentation actives during coseismic slip (Papa et al., 2018). (2) I*n situ* fragmentation occurs when the dynamic rupture tip propagates through the rock resulting in fragmentation (Austrheim et al., 1996, 2017; Petley-Ragan et al., 2018, 2019; Incel et al. 2019; Campbell and Menegon, 2022). To distinguish between the two hypotheses, the relative timing of shearing versus shattering is crucial. Our data shows that shattered grains are not exclusively seen in direct vicinity or within pseudotachylyte veins themselves (Fig. 3B), placing the timing of shattering before frictional slip. This interpretation is supported by other field studies (e.g., Mancktelow et al. 2022) and by experimental results of Incel et al. (2019) who interpreted garnet grains to be shattered as the rupture tip passes through the damage zone. Shearing behind the rupture tip results in these experiments in the formation of melt. Further support stems from plagioclase exhibiting *in situ* fragmentation while deformation twins occur within clinopyroxenes, both features that have been linked to high transient stresses at propagating rupture tips (e.g., Trepmann and Stöckhert, 2001).

The exact underlying mechanisms responsible for *in situ* mineral shattering/pulverization by dynamic rupture propagation remains unclear, at least for situations where this occurs at high confining pressures. While there is a consensus that pulverization in the vicinity of shallow faults is directly related to tensile stresses (Griffith et al., 2018), for deep faults the relative importance of compressive versus tensile stresses remains debated. The importance of tensile stresses has been emphasized by Incel et al. (2019) and Griffith et al. (2018). Griffith et al. (2018) concludes that the elastic strain energy which is directly linked to material strength and fracture toughness is at the core of fragmentation in a tensile regime. Toughness is a measure of a material's resistance to

fracture when subjected to stress. It is defined as the energy required to break a material. Materials with high toughness can absorb a large amount of energy before breaking; hence in engineering materials with high toughness are often used in applications where impact resistance is important (e.g. Spray, 2010 and references therein). Ductility, in contrast, is a material's ability to deform before breaking. Thus, to be able to fracture a material, its ductility needs to decrease. Both, toughness and ductility are not state constants; they change dynamically if deformation occurs by dislocation movement. Strain hardening decreases ductility and increases the elastic strain energy of the deformed material which in turn is the reason for a decrease in toughness (e.g. Incel et al., 2019 and references therein). For example, crystal plastically deformed grains that exhausted their easy slip system, and/or exhibit a high degree of dislocation entanglement preventing further dislocation generation or movement will become increasing prone to fracturing. At the same time, the tensile strength of geological materials is about a third of its compressive strength, hence fragmentation under tensile stress requires a third of the stress magnitude than under compression. Dislocation density is therefore an appropriate proxy for elastic strain energy as a dislocation distorts a lattice elastically (Fig. 7A; EBSP insets). In cases, where climb is not activated, i.e. low temperature plasticity, recovery is minor resulting in a direct proportionality of dislocation density and stored elastic energy. Our analyses show a positive correlation between fragmentation and geometrically necessary dislocation

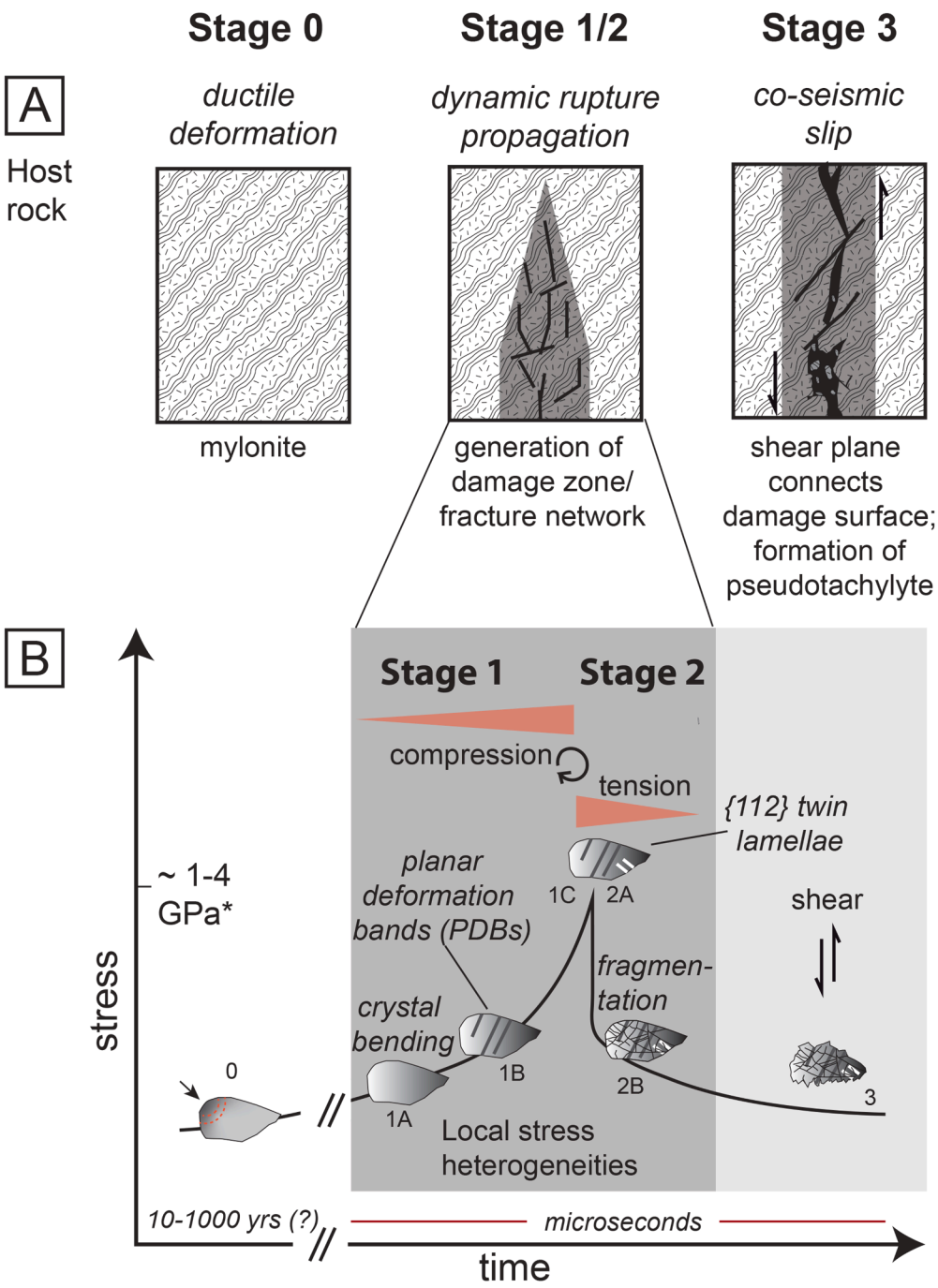

Fig. 8. Schematic conceptual model depicting the evolution of the host rock (A) and the damage zone (B) before (Stage 0), during (Stage 1 and 2) and in the wake of dynamic earthquake rupture propagation (Stage 3); processes are noted in *italic*; please refer to section 5.5. for more detail. In (B) arrow for stage 0 highlights indentation; *stress estimates are indicative only as values are taken from impact related shock pressure estimates (see section 5.2. for more details).

density (GND; Fig. 7). This means that those grains that are expected to have had high stored elastic energy based on their GND, have lower toughness, thus lower resistance to fracturing. These grain fragment *in-situ* during tensile stresses in wake of the propagating rupture tip, similar to rarefraction during shock deformation. The fact that only some of the grains were subject to fragmentation suggests that mean tensile stresses must have been below the tensile strength of zircon; thus, stored elastic energy played a major role in fragmentation. This is consistent with results of Incel et al. (2019) who concluded that strain rather kinetic energy triggered fragmentation. Toffol et al. (2024) show similar ranges of dislocation densities as observed here (Fig. 7) for their pulverized garnet associated with a pseudotachylyte. Our results are consistent with the proposed model that PDBs may develop into {112} twin lamellae during the passage of the rarefaction wave under negative, extension pressure (Moser et al. 2011), however in our case these are not shock related rarefraction waves, but tensile stresses associated with dynamic earthquake rupture propagation.

5.4. Shear and frictional melting

The spatial association of the pseudotachylyte with the damage zone, suggests that formation of pseudotachylyte was after damage formation and aided by the presence of the damage zone. The damaged rock is highly fractured and therefore has a large number of rough surfaces that can be activated during seismic slip (e.g., Magloughlin, 1992; Spray, 2010). Observations suggest that frictional slip postdates both compression at the propagating tip and tensile stresses in the wake of this propagation. This fast displacement of wall rock results in pseudotachylyte formation in the damage zone (Fig. 8A). The suggested sequence of events is consistent with observations from experimental results of Incel et al. (2019) and interpretations based on microstructural features form natural examples of deep earthquakes in dry rocks (Petley-Ragan et al., 2018, Campbell and Menegon, 2022) who interpreted frictional slip occurred after *in-situ* fragmentation along selected surfaces. Interestingly, sheared fragmented zircons are dominantly observed in the damaged zone. This suggests that within the melt(now pseudotachylyte)-clast areas slip was taken up mainly by the melt; thus, the fragmented zircon grains largely stay intact preserving the *in-situ* fragmentation except when at the border to a pseudotachylyte vein. In contrast, within the damage zone fragmented and displaced zircons are common, hence within the damage zone slip was accommodated by slip along short preexisting failure planes without producing seismic slip and local melting.

5.5. Zircon microstructures reveal succession of transient events during rupture: A Model

Our large dataset with a wealth of studied deformation features and their relative timing of their formation allows us to define a sequence of transient events and link these to underlying microphysical processes (Fig. 8):

Stage 0: Initial stage of ductile deformation

Deformation at mid-crustal levels occurs within localized mylonitic to ultramylonitic shear zones where zircons remain intact and show little lattice distortions concentrated at grain boundaries (e.g., Fig. 8B, 0, indentation).

Stage 1: Rupture tip propagation triggers damage zone formation and rapid crystal plastic deformation of zircon

Intermittently, high stresses result in rupture tips propagating within the mid crust. Reches and Dewers (2005) showed that at the tip of a propagating dynamic shear fracture extremely high pressures can occur and result in the formation of a damage zone (Fig. 8A). Unfortunately, due to the complicated vein network observed (Figs. 1D, 2A,B, 3A) the predicted asymmetry of stresses could not be assessed. At the rupture tip locally high stresses are generated and induce instantaneous low temperature dislocation production within zircon resulting in the observed crystal bending throughout grains with activation of a high stress slip system and formation of planar deformation bands (PDBs; Figs. 3-5). As PDBs are cutting continuous crystal bending, bending must have come first (Fig. 8; 1A, 1B). This is in line with the fact that high dislocation production results in strain hardening (e.g., Mecking and Kocks, 1981); during continued high stresses PDBs may form as the ability of the crystal to bend continuously is exhausted. Locally stresses reach levels that are sufficient to produce {112} twin lamellae (Fig. 8B, 1C) especially in grains that have already accumulated a high number of dislocations such as those seen with PDBs (Fig. 7A; note high GNDs for twinned grain; marked in red). Comparison of observed zircon microstructures with those reported from impact structures provide indicative stress levels in the order of a few GPa (see section 5.2. for detailed discussion). Stress must have been highly heterogeneous as evidenced by the high variability of microstructures in grains in close proximity. Such highly variable stresses during dynamic shear fracture tip propagation have been proposed by Reches and Dewers (2005). Consequently, we related both damage zone formation and observed crystal plastic deformation features to compressive stresses at the rupture tip.

Stage 2: Tension in wake of propagating rupture tip causes in-situ fragmentation

After compressional stresses at the propagating rupture tip pass through the rock, *in-situ* zircon fragmentation is triggered in those grains characterized by very lattice distortion and high dislocation densities (Fig. 5, 7A). This sequence of events is supported by the fact that fragments not only exhibit features of intense crystal plastic deformation as described above but importantly follow their shape (Fig. 4D) or cut across them (Fig. 5). The characteristics of the fragmented grains (Fig. 5) resemble reported occurrences of fragmented, shattered/pulverized minerals which have been associated with seismic faulting: e.g. garnet (Austrheim et al., 2017, Trepmann and Stöckhert, 2002; Papa et al., 2018, Toffol et al., 2024); feldspar (Okudaira et al., 2017) and clinopyroxene (Campbell and Menegon, 2022). In these cases, fragmentation is interpreted to occur during coseismic slip as the consequence of the instantaneous rise and drop of stresses due to either synseismic loading (e.g., Trepmann and Stöckhert, 2002) or thermal shock (Papa et al., 2018). According to Reches and Dewers (2005) during dynamic shear fracture tip propagation stresses may not only be highly variable but alternating between volumetric contraction and expansion. Such volumetric contraction and expansion within microseconds may explain the observed fragmentation which necessitates near instantaneous stress rise and drop. The spatial association of the damage zone, microstructures suggesting local stress variations, and common *in-situ* fragmentation is consistent with the mechanics of a propagating dynamic shear fracture tip. Pressure heterogeneity may also explain the occurrence of the two groups of *in-situ* fragmentation as fragmentation with variable absolute differences in contractional versus extensional pressure. Fragmentation with little rotation between fragments (Fig. 5A, 5C) requires lower pressure release than those with high relative rotations which must have been subject to instantaneously high-pressure release to allow for the space necessary to rotate fragments a higher degree (Fig. 5B). Importantly, zircons with very high dislocation densities and thus very high stored elastic energy are “pre-conditioned” for fragmentation, as the stored elastic stresses result in a decrease of their tensile strength; hence these grains fragment during tensile stresses (Fig. 8B, 2b). Grains with planar deformation may be reworked under tension developing {112} twin lamellae (Moser et al. 2011).

Stage 3: Shear displacement along connected network of damage fracture planes

Deformation changes from alternating stresses related to the instantaneous fracture tip propagation to displacement of the rock volume along a network of damage related fractures. Displacement along preexisting brittle failure surfaces is supported by the observed shearing of fragmented zircon (Figs. 3, 5) to form fragmented and displaced grains (Fig. 8B, 3).

6. Conclusions

Our large dataset of zircon microstructures developed in and in the vicinity of pseudotachylytes present in the IVZ of the Western Alps confirms that earthquakes can be triggered by dynamic rupture not only in very dry, high confining pressure conditions but also at mid-crustal conditions in the presence of hydrous phases such as amphibole. Our results contrast the suggested mechanisms of mid-crustal earthquake generation through high stress, high strain rate ductile deformation.

Our study highlights the importance of transient events. Rupture tip propagation results in damage zone formation and triggers dislocation generation and a range of microstructures with high lattice distortion by low temperature plasticity throughout whole grains which contrasts the localized deformation of zircons deformed at tectonic strain rates in the ductile field. Distortions include planar deformation bands, high lattice distortion with activation of several slip systems and {112} twin lamellae. Compressive stresses are highly heterogeneous based on the heterogeneous nature of the rock deformed and can reach stresses on the order of a few GPa. Transient tensile stresses in the wake of the propagating rupture tip result in local grain fragmentation/pulverization. High dislocation densities in pulverized zircon suggests a causal relationship as high dislocation densities decrease the effective tensile strength of the deformed zircons. Therefore, grains with sufficiently high dislocation densities, exhibit sufficiently low tensile strength to fragment in situ during these transient tensile stresses. Subsequent shear along a network of pre-existing damage fracture planes allows for seismic slip and pseudotachylyte formation.

Our study shows that zircon is a very good stress indicator expanding its value from geochronology and impact recognition to tectonics and associated processes.

CRediT authorship contribution statement

Sandra Piazolo: Writing – review & editing, Writing – original draft, Resources, Project administration, Methodology, Investigation, Formal analysis, Data curation, Conceptualization. **Antonio Langone:** Writing – review & editing, Validation, Methodology, Investigation, Funding acquisition, Formal analysis, Data curation, Conceptualization.

Declaration of competing interest

The authors declare the following financial interests/personal relationships which may be considered as potential competing interests:

Antonio Langone reports financial support was provided by Consiglio Nazionale delle Ricerche. Reports a relationship with that includes:. Has patent pending to. If there are other authors, they declare that they have no known competing financial interests or personal relationships that could have appeared to influence the work reported in this paper.

Acknowledgements

The following projects partially funded this research: PRIN2017 “Micro to Macro - how to unravel the nature of the large magmatic events” (20178LPCPW- Langone Antonio); Short Term Mobility grant (2017; A. Langone) of the CNR (Italy). SP acknowledges the Cheney Fellowship funding (2020-2025) and help by D. Morgan during optical-microscope CL analysis.

Supplementary materials

Supplementary material associated with this article can be found, in the online version, at doi:10.1016/j.epsl.2026.119858.

Data availability

Data will be made available on request.

References

Aldrighetti, S., Pennacchioni, G., Di Toro, G., 2025. Earthquake dynamics from pseudotachylyte microstructure. Earth Planet. Sci. Lett. 663, 119424.
Austrheim, H., Corfu, F., 2009. Formation of planar deformation features (PDFs) in zircon during coseismic faulting and an evaluation of potential effects on U-Pb systematics. Chem. Geol. 261, 24–30.
Austrheim, H., Erambert, M., Boundy, T.M., 1996. Garnet recording deep crustal earthquakes. Earth Planet. Sci. Lett. 139, 223–238.
Austrheim, H., Dunkel, K.G., Plümper, O., Ildefonse, B., Liu, Y., Jamtveit, B., 2017. Fragmentation of wall rock garnets during deep crustal earthquakes. Sci. Adv., e1602067
Braeck, S., Podladchikov, Y.Y., 2007. Spontaneous thermal runaway as an ultimate failure mechanism of materials. Phys. Rev. Lett. 98. https://doi.org/10.1103/PhysRevLett.98.095504.
Borthwick, V.E., Piazolo, S., 2010. Post-deformational annealing at the subgrain scale: Temperature dependent behaviour revealed by in-situ heating experiments on deformed single crystal halite. J. Struct. Geol. 32, 982–996.
Campbell, L.R., Menegon, L., 2022. High Stress deformation and short-term thermal pulse preserved in pyroxene microstructures from exhumed lower crustal seismogenic faults (Lofoten, Norway). J. Geophys. Res.: Solid Earth 127, e2021JB023616. https://doi.org/10.1029/2021JB023616.
Cavosie, A.J., Erickson, T.M., Timms, N.E., 2015. Nanoscale records of ancient shock deformation: reidite (ZrSiO4) in sandstone at the Ordovician Rock Elm impact crater. Geology 43, 315–318.
Corvò, S., Maino, M., Piazolo, S., Kylander-Clark, A.R.C., Seno, S., Langone, A., 2023. Crystal plasticity and fluid availability govern the ability of titanite to record the age of deformation. Earth Planet. Sci. Lett. 620, 118349.
Corvò, S., Montemagni, C., Zanchetta, S., Langone, A., 2025. Intermittent brittle and ductile deformation as recorded by dating of Ultramylonites and Pseudotachylytes in extending continental crust (Ivrea-Verbano Zone, Italy). Terra Nova. https://doi.org/10.1111/ter.12775.
Cox, M.A., Cavosie, A.J., Bland, P.A., Miljkovic, K., Wingate, M.T.D., 2018. Microstructural dynamics of central uplifts: reidite offset by zircon twins at the Woodleigh impact structure. Aust. Geol. 46, 983–986. https://doi.org/10.1130/G45127.1.
Degli Alessandrini, G., 2018. PhD thesis. School of Geography, Earth and Environmental Sciences; University of Plymouth.
Doan, M.-L., Gary, G., 2009. Rock pulverization at high strain rate near the San Andreas fault. Nat. Geosci 2, 709–712.
Erickson, T.M., Cavosie, A.J., Moser, D.E., Barker, I.R., Radovan, H.A., 2013. Correlating planar microstructures in shocked zircon from the Vredefort Dome at multiple scales: Crystallographic modeling, external and internal imaging, and EBSD structural analysis. Am. Mineral. 98, 53–65. https://doi.org/10.2138/am.2013.4165.
Erickson, T.M., Pearce, M.A., Reddy, S.M., Timms, N.E., Cavosie, A.J., Bourdet, J., Rickard, W.D.A., Nemchin, A.A., 2017. Microstructural constraints on the mechanisms of the transformation to reidite in naturally shocked zircon. Contrib. Mineral. Petrol. 172, 2. https://doi.org/10.1007/s00410-016-1322-0.
Ewing, T.A., Rubatto, D., Beltrando, M., Hermann, J., 2015. Constraints on the thermal evolution of the Adriatic margin during Jurassic continental break-up: U–Pb dating of rutile from the Ivrea-Verbano Zone. Italy. Contrib. Miner. Pet. 169, 44. https://doi.org/10.1007/s00410-015-1135-6.
Faulkner, D.R., Mitchell, T.M., Jensen, E., Cembrano, J., 2011. Scaling of fault damage zones with displacement and the implications for fault growth processes. J. Geophys. Res.: Solid Earth 116.
Griffith, W.A., Julien St., R.C., Ghaffari, H.O., Barber, T.J., 2018. A tensile origin for fault rock pulverization. J. Geophys. Res.: Solid Earth 123, 7055–7073. https://doi.org/10.1029/2018JB015786.
Incel, S., Hilairet, N., Labrousse, L., John, T., Deldicque, D., Ferrand, T.P., Wang, Y., Morales, L., Schubnel, A., 2017. Laboratory earthquakes triggered during eclogitization of lawsonite-bearing blueschist. Earth Planet. Sci. Lett. 459, 320–331. https://doi.org/10.1016/j.epsl.2016.11.047.
Incel, S., Schubnel, A., Renner, J., John, T., Labrousse, L., Hilairet, N., Freeman, H., Wang, Y., Renard, F., Jamtveit, B., 2019. Experimental evidence for wall-rock pulverization during dynamic rupture at ultra-high pressure conditions. Earth Planet. Sci. Lett. 528, 115832.
Jamtveit, B., Ben-Zion, Y., Renard, F., Austrheim, H., 2018. Earthquake-induced transformation of the lower crust. Nature 556 (7702), 487–491. https://doi.org/10.1038/s41586-018-0045-y.
John, T., Medvedev, S., Rüpke, L.H., Andersen, T.B., Podladchikov, Y.Y., Austrheim, H., 2009. Generation of intermediate-depth earthquakes by self-localizing thermal runaway. Nat. Geosci. 2, 137–140. https://doi.org/10.1038/ngeo419.

Jones, G., Moser, D.E., Shieh, S.R., 2018. A numerical model for twin nucleation in shocked zircon and comparison with natural samples. Geophys. Res. Lett. 45. https://doi.org/10.1029/2018GL079081.
Kelemen, P.B., Hirth, G., 2007. A periodic shear-heating mechanism for intermediate-depth earthquakes in the mantle. Nature 446, 787–790. https://doi.org/10.1038/nature05717.
Kovaleva, E., Klötzli, U., Habler, G., Libowitzky, E., 2014. Finite lattice distortion patterns in plastically deformed zircon grains. Solid Earth 6, 1799–1861.
Kovaleva, E., Klötzli, U., Habler, G., Wheeler, J., 2015. Planar microstructures in zircon from paleo-seismic zones. Am. Mineral. 100, 1834–1847.
Langone, A., Zanetti, A., Daczko, N.R., Piazolo, S., Tiepolo, M., Mazzucchelli, M., 2018. Zircon U-Pb Dating of a Lower Crustal Shear Zone: A Case Study From the Northern Sector of the Ivrea-Verbano Zone (Val Cannobina, Italy). Tectonics 37. https://doi.org/10.1002/2017TC004638.
Leroux, H., Reimold, W.U., Koeberl, C., Hornemann, U., Doukhan, J.C., 1999. Experimental shock deformation in zircon: a transmission electron microscopic study. Earth Planet. Sci. Lett. 169, 291–301.
Magloughlin, J.F., 1989. Nature and significance of pseudotachylite from the Nason Terrane, North Cascade Mountains. Wash. J. Struct. Geol. 11, 907–917.
Magloughlin, J.F., 1992. Microstructural and chemical changes associated with cataclasis and frictional melting at shallow crustal levels: the cataclasite-pseudotachylyte connection. Tectonophysics 204, 243–260.
Mancktelow, N.S., Camacho, A., Pennacchioni, G., 2022. Time-lapse record of an earthquake in the dry felsic lower continental crust preserved in a pseudotachylyte-bearing fault. J. Geophys. Res.: Solid Earth 127, e2021JB022878.
Mecking, H., Kocks, U.F., 1981. Kinetics of flow and strain-hardening. Acta Metall. 29, 1865–1875.
Menegon, L., Pennacchioni, G., Malaspina, N., Harris, K., Wood, E., 2017. Earthquakes as precursors of ductile shear zones in the dry and strong lower crust. Geochem. Geophys. Geosystems 18, 4356–4374. https://doi.org/10.1002/2017GC007189.
Montalvo, P.E., Cavosie, A.J., Kirkland, C.L., Evans, N.J., McDonald, B.J., Talavera, C., Erickson, T.M., Lugo-Centeno, C., 2018. Detrital shocked zircon provides first radiometric age constraint (<1472 Ma) for the Santa Fe impact structure, New Mexico, USA. GSA Bull. 131, 845–863. https://doi.org/10.1130/B31761.1.
Morozova, I., Shieh, S.R., Moser, D.E., Barker, I.R., Hanchar, J.H., 2017. Strength and Deformation of Zircon at Crustal and Mantle Pressures. In: Moser, D.E., Corfu, F., Darling, J.R., Reddy, S.M., Tait, K. (Eds.), Microstructural Geochronology - Planetary Records Down to Atom Scale. AGU - Wiley, pp. 169–182.
Moser, D.E., Cupelli, C.L., Barker, I.R., Flowers, R.M., Bowman, J.R., Wooden, J., Hart, J. R., 2011. New zircon shock phenomena and their use for dating and reconstruction of large impact structures revealed by electron nanobeam (EBSD, CL, EDS) and isotopic U–Pb and (U–Th)/He analysis of the Vredefort dome. Can. J. Earth Sci.; 48, 117–139. https://doi.org/10.1139/E11-011.
Obata, M., Karato, S.-I., 1995. Ultramafic pseudotachylite from the Balmuccia peridotite, Ivrea-Verbano zone, northern Italy. Tectonophysics 242, 313–328.
Okazaki, K., Hirth, G., 2016. Dehydration of lawsonite could directly trigger earthquakes in subducting oceanic crust. Nature 530, 81–84. https://doi.org/10.1038/nature16501.
Okudaira, T., Shigematsu, N., Harigane, Y., Yoshida, K., 2017. Grain size reduction due to fracturing and subsequent grain-size-sensitive creep in a lower crustal shear zone in the presence of a CO2-bearing fluid. J. Struct. Geol. 95, 171–187.
Papa, S., Pennacchioni, G., Angel, R.J., Faccenda, M., 2018. The fate of garnet during (deep-seated) coseismic frictional heating: The role of thermal shock. Geology 46, 471–474. https://doi.org/10.1130/G40077.1.
Papa, S., Pennacchioni, g., Menegon, L., Thielmann, M., 2020. High-stress creep preceding coseismic rupturing in amphibolite-facies ultramylonites. Earth Planet. Sci. Lett. 541, 116260.
Petley-Ragan, A., Dunkel, K.G., Austrheim, H., Ildefonse, B., Jamtveit, B., 2018. Microstructural records of earthquakes in the lower crust and associated fluid-driven metamorphism in plagioclase-rich granulites. J. Geophys. Res. Solid Earth 123, 3729–3746. https://doi.org/10.1029/2017JB015348.
Petley-Ragan, A., Ben-Zion, Y., Austrheim, H., Ildefonse, B., Renard, F., Jamtveit, B., 2019. Dynamic earthquake rupture in the lower crust. Sci. Adv. 5, eaaw0913.
Piazolo, S., Austrheim, H., Whitehouse, M., 2012. Brittle-ductile microfabrics in naturally deformed zircon: Deformation mechanisms and consequences for U-Pb dating. Am. Mineral. 97, 1544–1563. https://doi.org/10.2138/am.2012.3966.
Piazolo, S., Montagnat, M., Grennerat, F., Moulinec, H., Wheeler, J., 2015. Effect of local stress heterogeneities on dislocation fields: Examples from transient creep in polycrystalline ice. Acta Mater. 90, 303–309.
Pittarello, L., Pennacchioni, G., Di Toro, G., 2012. Amphibolite-facies pseudotachylytes in Premosello metagabbro and felsic mylonites (Ivrea Zone, Italy). Tectonophysics 580, 43–57.
Raleigh, C.B., Paterson, M.S., 1965. Experimental deformation of serpentinite and its tectonic implications. J. Geophys. Res. 70, 3965–3985. https://doi.org/10.1029/JZ070i016p03965.
Reches, Z., Dewers, T., 2005. Gouge formation by dynamic pulverization during earthquake rupture. Earth Planet. Sci. Lett. 235, 361–374.
Reddy, S.T., Timms, N.E., Trimby, P., Kinny, P.D., Buchan, C., Blake, K., 2006. Crystal-plastic deformation of zircon: a defect in the assumption of chemical robustness. Geology 34, 257–260.
Rowe, C.D., Griffith, W.A., 2015. Do faults preserve a record of seismic slip: a second opinion. J. Struct. Geol. 78, 1–26.
Rutter, E.H., Brodie, K.H., Evans, P.J., 1993. Structural geometry, lower crustal magmatic underplating and lithospheric stretching in the Ivrea-Verbano Zone, Northern Italy. J. Struct. Geol. 15, 647–662.
Scholz, C.H., 2002. The Mechanics of Earthquakes and Faulting, 2nd ed. Cambridge University Press, Cambridge, p. 471.
Sibson, R.H., 1975. Generation of pseudotachylyte by ancient seismic faulting. Geophys. J. R. Astron. Soc. 43, 775–794.
Spray, J.G., 2010. Frictional melting processes in planetary materials: from hypervelocity impact to earthquakes. Annu. Rev. Earth Planet. Sci. 38, 221–254. https://doi.org/10.1146/annurev.earth.031208.100045.
Techmer, K.S., Ahrendt, H., Weber, K., 1992. The development of pseudotachylyte in the Ivrea-Verbano Zone of the Italian Alps. Tectonophysics 204, 307–322.
Thielmann, M., Rozel, A., Kaus, B.J.P., Ricard, Y., 2015. Intermediate-depth earth-quake generation and shear zone formation caused by grain size reduction and shear heating. Geology 43, 791–794. https://doi.org/10.1130/G36864.1.
Thomson, O.A., Cavosie, A.J., Moser, D.E., Barker, I., Radovan, H.A., French, B.A., 2014. Preservation of detrital shocked minerals derived from the 1.85 Ga Sudbury impact structure in modern alluvium and Holocene glacial deposits, 126. Geological Society of America Bulletin, pp. 720–737.
Timms, N.E., Kinny, P.D., Reddy, S.T., 2006. Enhanced diffusion of Uranium and Thorium linked to crystal plasticity in zircon. Geochem. Trans. 7, 10.
Timms, N.E., Erickson, T.M., Pearce, M.A., Cavosie, A.J., Schmieder, M., Tohver, E., Reddy, S.T., Zanetti, M.R., Nemchin, A.A., Wittmann, A., 2017. A pressure-temperature phase diagram for zircon at extreme conditions. Earth-Sci. Rev. 165, 185–202.
Toffol, G., Pennacchioni, G., Menegon, L., Wallis, D., Faccenda, M., Camacho, A., Bestmann, M., 2024. On-fault earthquake energy density partitioning from shocked garnet in an exhumed seismic midcrustal fault. Sci. Adv. 10, eadi8533.
Tommasi, A., Langone, A., Padrón-Navarta, J.A., Zanetti, A., Vauchez, A., 2017. Hydrous melts weaken the mantle, crystallization of pargasite and phlogopite does not: Insights from a petrostructural study of the Finero peridotites, southern Alps. Earth Planet. Sci. Lett. 477, 59–72.
Trepmann, C.A., 2008. Shock effects in quartz: Compression versus shear deformation—An example from the Rochechouart impact structure. Fr. Earth Planet. Sci. Lett. 267, 322–332.
Trepmann, C.A., Stöckhert, B., 2001. Mechanical twinning of jadeite- an indication of synseismic loading beneath the brittle-ductile transition. Int. J. Earth Sci. 90, 4–13.
Trepmann, C.A., Stöckhert, B., 2002. Cataclastic deformation of garnet: a record of synseismic loading and postseismic creep. J. Struct. Geol. 24, 1845–1856.
Ueda, T., Obata, M., Di Toro, G., Kanagawa, K., Ozawa, K., 2008. Mantle earthquakes frozen in mylonitized ultramafic pseudotachylytes of spinel-lherzolite facies. Geology 36, 607–610.
van Schrojenstein Lantman, H.W., Carvalho, P.A., Wallis, D., Menegon, L., 2025. Residual stress in diopside: insight into localized transient high stress in seismogenic faults in the lower crust, Lofoten, Norway. J. Struct. Geol. 200, 105517.
Wheeler, J., Mariani, E., Piazolo, S., Prior, D.J., Trimby, P., Drury, M.R., 2009. The weighted Burgers vector: a new quantity for constraining dislocation densities and types using electron backscatter diffraction on 2D sections through crystalline materials. J. Microsc. 233, 482–494.
Wheeler, J., Piazolo, S., Prior, D.J., Trimby, P.W., Tielke, J.A., 2024. Using crystal-lattice distortion data for geological investigations: the weighted Burgers vector method. J. Struct. Geol. 179, 105040.
White, J.C., 2012. Paradoxical pseudotachylyte e Fault melt outside the seismogenic zone. J. Struct. Geol. 38, 11e20.